**Atmospheric
Chemistry
and Physics**
Discussions

Open Access

Identification of gravity wave sources using reverse ray tracing over Indian region

**M. Pramitha[1], M. Venkat Ratnam[1], A. Taori[1], B. V. Krishna Murthy[2],
D. Pallamraju[3], and S. Vijaya Bhaskar Rao[4]**

[1]National Atmospheric Research Laboratory (NARL), Gadanki, India
[2]B1, CEBROS, Chennai, India
[3]Physical Research Laboratory (PRL), Ahmadabad, India
[4]Department of Physics, Sri Venkeswara University, Tirupati, India

Title Page

Abstract	Introduction
Conclusions	References
Tables	Figures

|◄ | ►|

◄ | ►

Back | Close

Full Screen / Esc

Printer-friendly Version

Interactive Discussion

Abstract

Reverse ray tracing method is successfully implemented for the first time in the Indian region for identification of the sources and propagation characteristics of the gravity waves observed using airglow emissions from Gadanki (13.5° N, 79.2° E) and Hyderabad (17.5° N, 78.5° E). Wave amplitudes are also traced back for these wave events by including both radiative and diffusive damping. Background temperature and wind data obtained from MSISE-90 and HWM-07 models, respectively, are used for the ray tracing. For Gadanki region suitability of these models is tested. Further, a climatological model of background atmosphere for Gadanki region has been developed using a long-term of nearly 30 years of observations available from a variety of ground-based (MST radar, radiosonde, MF radar), rocket-, and satellite-borne measurements. For considering real-time atmospheric inputs, ERA-Interim products are utilized. By this reverse ray method, the source locations for nine wave events could be identified to be in the upper troposphere, whereas, for five other events the waves seem to have been ducted in the mesosphere itself. Uncertainty in locating the terminal points in the horizontal direction is estimated to be within 50–100 and 150–300 km for Gadanki and Hyderabad wave events, respectively. This uncertainty arises mainly due to non-consideration of the day-to-day variability in tidal amplitudes. As no convection in-and-around the terminal points are noticed, it is unlikely to be the source. Interestingly, large ($\sim 9\,\mathrm{m\,s^{-1}}$ $\mathrm{km^{-1}}$) vertical shear in the horizontal wind is noted near the ray terminal points (at 10–12 km altitude) and is identified to be the source for generating the nine wave events. Conditions prevailing at the terminal points for each of the 14 events are also provided. These events provide leads to a greater understanding of the tropical lower and upper atmospheric coupling through gravity waves.

1 Introduction

Atmospheric gravity waves (GWs) play an important role in the middle atmospheric structure and dynamics. They transport energy and momentum from the source region (mainly troposphere) to the upper atmosphere. When encountered with critical level, they are dissipated by transferring energy and momentum to the mean flow leading to changes in the thermal structure of the atmosphere (Fritts and Alexander, 2003). Several sources are identified for the generation of GWs which include, tropical deep convection through pure thermal forcing by latent heat release which can excite these waves with vertical scales comparable to the heating depth (Alexander et al., 1995; Piani et al., 2000; Fritts and Alexander 2003; Fritts et al., 2005), mechanical oscillator effect (Clark et al., 1986; Fovell et al., 1992), obstacle effect (Clark et al., 1986; Vincent and Alexander, 2000), topography (Lilly and Kennedy, 1973; Nastrom and Fritts, 1992; Alexander et al., 2010), geostrophic adjustment mainly in high latitudes (Suzuki et al., 2013) and vertical shear in horizontal winds (Fritts and Alexander, 2003). In general, significant progress has been made in the understanding of the physical processes for generating the spectrum of GWs through both observations and modeling. However, identification of the exact sources for the generation of GWs and their parameterization in the models still remain a challenge.

In order to identify the gravity wave sources, hodograph analysis has been widely used. This method is applicable only for medium and low frequency waves, as for the high frequency GWs the hodograph would not be an ellipse but nearly a straight line. Further, as it assumes monochromatic waves, it is not always applicable in the real atmosphere. Notwithstanding this limitation, using this method convection and vertical shear have been identified as the possible sources of the observed medium and low frequency GWs in the troposphere and lower stratosphere over many places (e.g., Venkat Ratnam et al., 2008). It becomes difficult to apply this method for GWs that are observed in the MLT region where simultaneous measurements of temperatures (with wind) would not be available.

A more appropriate method in such cases is that of the ray tracing (Marks and Eckermann, 1995), which is widely being used to identify the sources of GWs observed at mesospheric altitudes. Several studies (Hecht et al., 1994; Taylor et al., 1997; Nakamura et al., 2003; Gerrard et al., 2004; Brown et al., 2004; Wrasse et al., 2006; Vadas et al., 2009 and references therein) have been carried out to identify the sources for the GWs observed in the mesosphere using airglow images. In carrying out such studies, important GW parameters, such as, periodicities and horizontal wavelengths (and sometimes vertical wavelengths when two imagers are simultaneously used) are directly derived. A major limitation in the ray tracing method is the non-availability of realistic information of the background atmosphere, which is difficult to obtain with available suite of instrumentation. Nevertheless, possible errors involved in identifying the terminal point of the waves with and without realistic background atmosphere have been estimated (e.g., Wrasse et al., 2006; Vadas et al., 2009).

Over the Indian region, several studies (Venkat Ratnam et al., 2008 and references therein) have been carried out for extracting GW parameters using various instruments (MST radar, Lidar and satellite observations). In a few studies (Kumar, 2006, 2007; Dhaka et al., 2002; Venkat Ratnam et al., 2008; Debashis Nath et al., 2009; Dutta et al., 2009) possible sources in the troposphere for their generation are identified which include convection, wind shear, and topography. In the present investigation, for the first time, reverse ray tracing method is successfully implemented to identify the sources of the GWs at mesospheric altitudes observed from an airglow imager located at Gadanki (13.5° N, 79.2° E) and from a balloon experiment which carried an ultraviolet imaging spectrograph from Hyderabad (17.5° N, 78.5° E).

2 Database

2.1 Airglow imager observations and methodology for extracting GW characteristics

The NARL Airglow Imager (NAI) located at Gadanki is equipped with 24 mm of Mamiya fish eye lens. It monitors OH, $O(^1S)$, and $O(^1D)$ emissions and has a 1024×1024 pixels CCD as the detector. The present field-of-view of NAI is 90° which avoids non-linearity arising at higher zenith angles. As the imager is optimized for best viewing at these 3 wavelengths, the best images of mesospheric waves are noted in the $O(^1S)$ emissions which originate at ~ 93–100 km (with a peak emission altitude of ~ 97 km). The exposure time used to measure the $O(^1S)$ emissions intensities was 70 s. After capturing the image it has been analyzed and corrected for the background brightness, star brightness and actual coordinates. More details of the NAI are discussed by Taori et al. (2013).

We have observed three wave events between 14:29–14:51, 15:44–15:50 and 20:45–21:17 UTC on 17 March 2012 (Fig. 1) and two wave events between 15:47–16:27 and 16:31–16:54 UTC on 19 March 2012 in the $O(^1S)$ airglow emission intensities. In these images crests of the waves are emphasized by yellow freehand lines and motion of the waves are apparent in the successive images shown one below the other. Red arrows indicate the direction of the propagation of the waves. Horizontal wavelengths of the GWs are determined by applying 2-D FFT to the observed airglow images. The periods of the GWs are estimated by applying 1-D FFT in time to the complex 2-D FFT in space. Direction of propagation and phase speed of GWs are identified using successive images. More details of the methodology for estimating the GW parameters from NAI observations are provided in Taori et al. (2013). Table 1 summarizes the GW parameters (along with the uncertainties) extracted for the five wave events (G1 to G5) mentioned above. In general, the waves corresponding to these events are moving north, north-west direction. Zonal (k) and meridional (l) wave numbers are calculated using the relations $k = k_h \cos \phi$ and $l = k_h \sin \phi$ where k_h is the horizontal wave

number and ϕ is the horizontal direction of propagation observed from the airglow imager. The vertical wavelengths are also calculated using the GW dispersion relation. The calculated zonal, meridional and vertical wavelengths are also provided in Table 1. The large vertical wavelengths (13.6 to 28.9 km) and smaller periods suggest that these are high frequency GWs.

2.2 Daytime wave characteristics in the MLT region obtained through optical emissions

A multi-wavelength imaging echelle spectrograph (MISE) is used to obtain daytime emission intensities of oxygen emissions at 557.7, 630.0 and 777.4 nm. MISE obtains high resolution spectra of daytime skies which are compared with the reference solar spectrum. The difference obtained between them yields information on the airglow emissions in the daytime. The details of the emission extraction process and calibration procedures of the emission intensities and the salient results obtained in terms of wave coupling of atmospheric regions that demonstrate the capability of this technique have been described elsewhere (Pallamraju et al., 2013; Laskar et al., 2013). In the present experiment, the slit oriented along the magnetic meridian enabled information on the meridional scale size of waves (λ_y) at O(^{1}S) emission altitude of $\sim$ 100 km (in the daytime). An ultraviolet imaging spectrograph with its slit oriented in the east-west direction was flown on a high-altitude balloon (on 8 March 2010) which provided information on the zonal scale sizes of waves (λ_x) using the OI 297.2 nm emissions that originate at $\sim$ 120 km. The details of the experiment and the wave characteristics in terms of λ_x, λ_y, λ_H (horizontal scale sizes), time periods (τ), propagation speeds (c_H) and propagation direction (θ_H) obtained by this instrument at a representative altitude of 100 km are described in detail in Pallamraju et al. (2014). Nine events from this experiment are considered in the present study for investigating their source regions and are marked as H1 to H9 in Table 1.

2.3 Outgoing long-wave radiation (OLR) and brightness temperature in the infrared band (IR BT) products

Satellite data of OLR/IR BT are used as proxy for tropical deep convection. In general, the daily NOAA interpolated OLR can be used to obtain information on synoptic scale convection. However, for local convection on smaller spatial and temporal scales, the IR BT data merged from all available geostationary satellites (GOES-8/10, METEOSAT-7/5 GMS) are obtained from Climate Prediction Center, National Centre for Environment Prediction (NCEP) (source: ftp://disc2.nascom.nasa.gov/data/s4pa/TRMM_ANCILLARY/MERG/). The merged IR BT with a pixel resolution of 4 km is available from 60° N–60° S. The data in the east–west begins from 0.082° E with grid increment of 0.03637° of longitude and that in the north–south from 59.982° N with grid increment of 0.03638° of latitude (Janowiak et al., 2001). The BT dataset is retrieved for every half an hour interval over a region of ±5° around Gadanki and Hyderabad on 17 March 2012 and 8 March 2010, respectively, to see whether any convective sources were present in these locations.

3 Reverse ray tracing method

The reverse ray tracing method (Lighthill, 1978; LeBlond and Mysak, 1978; Schoeberl, 1985), which is widely used to trace back to the GW sources is utilized in the present study. For ray tracing description to be valid for $\psi = \psi_0 e^{i\theta}$ (where ψ is the amplitude and θ is the phase) the phase has to vary rapidly when compared to the amplitude and the phase changes by 2π when it moves through one wavelength (Landau and Lifshitz, 1962). In an inhomogeneous anisotropic atmosphere, $\omega = \omega(\boldsymbol{k}, \boldsymbol{x})$, where $\omega, \boldsymbol{k}, \boldsymbol{x}$ are frequency, wave number vector and position vector, respectively. Using ray tracing theory, the equations describing the ray path and refraction of the wave vector along the

ray are given by:

$$\frac{\mathrm{d}x}{\mathrm{d}t} = \frac{\partial \omega}{\partial k} = c_g(k) \tag{1}$$

$$\frac{\mathrm{d}k}{\mathrm{d}t} = -\frac{\partial \omega}{\partial x} \tag{2}$$

5   The ray tracing equations for GW are derived (Jones, 1969; Eckermann, 1992; Marks and Eckermann, 1995; Vadas, 2009) using the dispersion relation:

$$\omega_{ir}^2 = \frac{N^2(k^2 + l^2) + f^2(m^2 + \alpha^2)}{k^2 + l^2 + m^2 + \alpha^2} \tag{3}$$

where $\omega_{ir} = \omega - kU - lV$ is the intrinsic frequency (frequency relative to the mean wind), U and V are the zonal and meridional winds and N is the Brunt–Väisälä frequency, k, l

10 and m are the wave number vectors components in the zonal, meridional and vertical directions, respectively. $f = 2\Omega \sin \phi$ is the coriolis parameter $\alpha = 1/2H$ and H is the density scale height of the atmosphere. The ray tracing equations for gravity waves propagating through 3-D space are given below:

$$\frac{\mathrm{d}x}{\mathrm{d}t} = U + \frac{k\left(N^2 - \omega_{ir}^2\right)}{\omega_{ir}\Delta} \tag{4}$$

15
$$\frac{\mathrm{d}y}{\mathrm{d}t} = V + \frac{l\left(N^2 - \omega_{ir}^2\right)}{\omega_{ir}\Delta} \tag{5}$$

$$\frac{\mathrm{d}z}{\mathrm{d}t} = -\frac{m\left(\omega_{ir}^2 - f^2\right)}{\omega_{ir}\Delta} \tag{6}$$

$$\frac{\mathrm{d}k}{\mathrm{d}t} = -k\frac{\partial U}{\partial x} - l\frac{\partial V}{\partial x} - \frac{1}{2\omega_{ir}\Delta}\left[\frac{\partial N^2}{\partial x}(k^2 + l^2) - \frac{\partial \alpha^2}{\partial x}\left(\omega_{ir}^2 - f^2\right)\right] \tag{7}$$

Title Page

Abstract | Introduction

Conclusions | References

Tables | Figures

◄ | ►

◄ | ►

Back | Close

Full Screen / Esc

Printer-friendly Version

Interactive Discussion

$$\frac{\mathrm{d}l}{\mathrm{d}t} = -k\frac{\partial U}{\partial y} - l\frac{\partial V}{\partial y} - \frac{1}{2\omega_{\mathrm{ir}}\Delta}\left[\frac{\partial N^2}{\partial y}(k^2+l^2) - \frac{\partial \alpha^2}{\partial y}\left(\omega_{\mathrm{ir}}^2 - f^2\right)\right] - \frac{f}{\omega_{\mathrm{ir}}\Delta}\frac{\mathrm{d}f}{\mathrm{d}y}(m^2+\alpha^2) \quad (8)$$

$$\frac{\mathrm{d}m}{\mathrm{d}t} = -k\frac{\partial U}{\partial z} - l\frac{\partial V}{\partial z} - \frac{1}{2\omega_{\mathrm{ir}}\Delta}\left[\frac{\partial N^2}{\partial z}(k^2+l^2) - \frac{\partial \alpha^2}{\partial z}\left(\omega_{\mathrm{ir}}^2 - f^2\right)\right] \quad (9)$$

where, $\Delta = k^2 + l^2 + m^2 + \alpha^2$ and U and V are the zonal and meridional velocity. Note that this ray tracing theory is applicable only when WKB approximation is valid. WKB approximation is valid whenever the WKB parameter, $\delta = \frac{1}{m^2}\left|\frac{\partial m}{\partial z}\right| \approx \left|\frac{1}{C_{\mathrm{gz}}m^2}\frac{\mathrm{d}m}{\mathrm{d}t}\right|$ is less than unity, where C_{gz} is the vertical group velocity.

In order to calculate the wave amplitude we used the wave action equation of the form

$$\frac{\partial A}{\partial t} + \nabla \cdot (C_{\mathrm{g}}A) = -\frac{2A}{\tau} \quad (10)$$

where $A = E/\omega_{\mathrm{ir}}$ represents the wave action density, C_{g} represents the group velocity vector and $E = \frac{\rho_0}{2}[\overline{u'^2} + \overline{v'^2} + \overline{w'^2} + N^2\overline{\zeta'^2}]$ represents the wave energy density being the sum of kinetic and potential energy components, as described by wave perturbations in zonal, meridional and vertical velocities (u', v', w'), and vertical displacement (ζ'). Here ρ_0 is the background density and τ is the damping time scale (Marks and Eckermann, 1995). Using the peak horizontal velocity amplitude along the horizontal wave vector we can calculate the wave action density using the equation:

$$A = \frac{1}{4}\frac{\rho_0|\hat{u}_\backslash\backslash|^2}{\omega_{\mathrm{ir}}}\left\{1 + \frac{f^2}{\omega_{\mathrm{ir}}^2} + \frac{N^2 + \omega_{\mathrm{ir}}^2}{N^2 - \omega_{\mathrm{ir}}^2}\left(1 - \frac{f^2}{\omega_{\mathrm{ir}}^2}\right)\right\} \quad (11)$$

In order to avoid the spatial integration in the wave action equation we can write Eq. (10) in terms of the vertical flux of wave action $F = C_{\mathrm{gz}}A$, where F is the vertical flux of

wave action and C_{gz} is vertical component of the group velocity. Assuming negligible contribution from the higher order terms, the Eq. (11) can be written as:

$$\frac{dF}{dt} = -\frac{2}{\tau}F \tag{12}$$

As a wave moves through the atmosphere, amplitude damping takes place which is mainly due to eddy diffusion and infrared radiative cooling by CO_2 and O_3. At higher altitudes (above about 100 km) molecular diffusion becomes important as compared to the eddy diffusion. We can calculate the damping rate due to diffusion using:

$$\tau_D^{-1} = D(k^2 + l^2 + m^2 + \alpha^2) \tag{13}$$

Where, $D = D_{Eddy} + D_{molecular}$, represents the sum of eddy and molecular diffusivities. In order to calculate the infrared radiative damping we used Zhu (1993) damping rate calculation method from 20–100 km. The total damping rate is calculated using the following equation:

$$\tau^{-1} = \frac{\tau_r^{-1}\left(\frac{1-f^2/\omega_{ir}^2}{1-\omega_{ir}^2/N^2}\right) + \tau_D^{-1}\left(1 + \frac{f^2}{\omega_{ir}^2} + \frac{1-f^2/\omega_{ir}^2}{N^2/\omega_{ir}^2-1} + Pr^{-1}\frac{1-f^2/\omega_{ir}^2}{1-\omega_{ir}^2/N^2}\right)}{\left\{1 + \frac{f^2}{\omega_{ir}^2} + \frac{N^2+\omega_{ir}^2}{N^2-\omega_{ir}^2}\left(1 - \frac{f^2}{\omega_{ir}^2}\right)\right\}} \tag{14}$$

where Pr represents the Prandtl number and we have taken $Pr = 0.7$. Note that for high frequency waves diffusion damping effect will be less.

4 Background atmosphere

In order to carryout reverse ray-trace analysis, information on background atmospheric parameters (U, V and T) is required right from the initial point (mesosphere) to the termination point (usually the troposphere). In general, no single instrument exists which

can probe the troposphere, stratosphere, and mesosphere simultaneously. Note that in order to trace the ray we require atmospheric parameters for a specified latitude-longitude grid. Since the observed wave events belong to high frequencies (GWs with short horizontal wavelengths), we require the background information at least for a grid size of $5° \times 5°$ around the Gadanki and Hyderabad regions. Thus, for information on temperature and density at the required grids, we used Extended Mass Spectrometer and Incoherent Scatter Empirical Model (MSISE-90) data (Hedin, 1991) from surface to 100 km with an altitude resolution of 0.1 km for $0.1° \times 0.1°$ grid in-and-around these locations. Note that the MSISE-90 model is an empirical model which provides temperature and density data from the surface to the thermosphere. For horizontal winds at these grids, we used the outputs from the Horizontal Wind Model (HWM-07) (Drob et al., 2008) data. This model has been developed by using a total of 60×10^6 observations available from 35 different instruments spanning 50 years. Further, long-term data available from a variety of instruments (MST radar, MF radar, Rocketsonde, radiosonde, HRDI/UARS and SABER/TIMED satellites) in-and-around ($\pm 5°$) Gadanki have been used to develop a background climatological model profiles of U, V, and T on monthly basis. Details of the data used to develop the background temperature and horizontal winds are provided in Table 2. Monthly mean contours of temperature, zonal and meridional winds obtained from the climatological model (hereafter referred to as the Gadanki model) are shown in Fig. 2. In general, major features of the background atmospheric structure for a typical tropical region can be noticed from this figure. Tropopause, stratopause, and mesopause altitudes are located at around 16–18, 48–52, and 98–100 km with temperatures 190–200, 260–270 and 160–170 K, respectively. Mesospheric semi-annual oscillation around 80–85 km is also visible (Fig. 2a). Tropical easterly jet at around 16 km during the Indian Summer Monsoon season (June-July-August) and semi-annual oscillation near the stratopause (and at 80 km with different phase) are also clearly visible in the zonal winds (Fig. 2b). Meridional winds do not exhibit any significant seasonal variation in the troposphere and stratosphere but large variability can be noticed in the mesosphere (Fig. 2c). These overall features

in the background temperature and winds match well with those reported individu-
ally while considering the different instruments discussed in detail in Kishore Kumar
et al. (2008a, b), respectively.

The profiles of T obtained from MSISE-90 model and U and V from HWM-07 for
17 March 2012 are shown in Fig. 3a–c, respectively. The Gadanki model mean tem-
perature profile for the month of March and the temperature profile obtained from
TIMED/SABER are also superimposed in Fig. 3a for comparison. A very good agree-
ment between the profiles can be noticed. The profiles of U and V obtained from the
Gadanki model for the month of March are also superimposed in Fig. 3b and c, re-
spectively. In general, a good match is seen between the Gadanki model and HWM-07
models up to the altitudes of stratopause. The differences between the two above the
stratopause could be due to tidal winds which have large amplitudes at mesospheric
altitudes. Though tidal amplitudes are already included in the HWM-07 model, their
day-to-day variability may be contributing to these differences. In order to avoid any
bias due to day-to-day variability of the tides at mesospheric altitudes, we have con-
sidered tidal amplitudes of 5, 10, 15 K and 10, 20, 30 m s^{-1} in temperature and winds,
respectively, at 97 km to represent day-to-day variability.

In general, troposphere is a highly dynamic region though the amplitudes of tides are
considerably low. In order to consider more realistic horizontal winds in the troposphere
and stratosphere, we further considered the ERA-Interim products (Dee et al., 2011).
This data is available at 6 h intervals with 1.5° × 1.5° grid resolution at 37 pressure lev-
els covering from surface (1000 hpa) to the stratopause ($\sim$ 1 hPa). The profiles of T,
U and V from ERA-Interim for 17 March 2012 for 12:00 UTC are also superimposed
in Fig. 3a–c, respectively. In general, good agreement between the other models and
ERA-Interim can be noticed particularly in V in the lower and upper levels except be-
tween 10 and 20 km. Summarizing, we have considered the following wind models: (1)
Era-Interim (from surface to 40 km) and HWM 07 models from 40–100 km, (2) Gadanki
model, (3) zero wind ($U = 0$ and $V = 0$). Using these background atmosphere profiles,
we calculated the relevant atmospheric parameters like N^2 and H. Profiles of T, U, and

V obtained using ERA-interim data products for 8 March 2010, 06:00 UTC over Hyderabad region are shown in Fig. 3d–f, respectively. T, U, and V profiles as obtained from MSISE-90 and from HWM-07 for the same day are also provided in the respective panels. The background atmospheres were considered for wave events over Hyderabad are considered in a manner similar to that mentioned above for Gadanki.

In order to calculate diffusive damping we used eddy diffusivity profiles for troposphere and lower stratosphere and mesosphere which are obtained using MST Radar (Narayana Rao et al., 2001) at Gadanki as shown in Fig. 4a. In the altitude regions where there was data gap, we extrapolated/interpolated the diffusivity profiles and the approximated profile with different analytical exponential functions is also shown in Fig. 4a. The eddy diffusivity profile of Hocking's (Hocking, 1991) that presented in Marks and Eckermann (1995) is also superimposed for comparison. Note that Hocking's profile corresponds mainly to mid latitudes. In general, eddy diffusivity is relatively higher in Hocking's profile than in the Gadanki profile. This same (Gadanki) profile is used for Hyderabad events also. In Fig. 4b molecular diffusivity is shown. It is seen that the molecular diffusivity exceeds the eddy diffusivity at altitudes > 80 km. We have taken into account molecular diffusivity also in the ray tracing calculation while considering the total diffusivity above 80 km and the total diffusivity profile is shown in Fig. 4b. Radiative and diffusive damping rates corresponding to Event G1 observed over Gadanki are shown in Fig. 4c for illustration. It is seen that radiative damping rate is higher than the diffusive damping rates below 95 km. This is so for the other 13 events (G2–G5 and H1–H9) as well.

5 Application of reverse ray tracing for the wave events

By using the background parameters and the ray tracing equations, we trace back the ray path(s) to identify the GW source region(s). We used Runge-kutta fourth order method for numerical integration at the time step of $\delta t = 100\,\mathrm{m}\,C_{gz}^{-1}$ where 100 m is the height step downwards from 97 km (the peak altitude of the airglow layer) and C_{gz} is

Identification of gravity wave sources using reverse ray tracing over Indian region

M. Pramitha et al.

the vertical group velocity. As the ray tracing theory is valid only when WKB approximation holds good, the ray integration is terminated whenever the WKB approximation is violated. We terminated the ray when (1) m^2 becomes negative, which means that the wave cannot propagate vertically, (2) intrinsic frequency < 0 or approaching zero, which means waves reached the critical layer and is likely to break beyond this value, (3) WKB parameter approaching values greater than one (beyond which WKB approximation breaks) and (4) vertical wave number becoming greater than 1×10^{-6} (approaching critical level) (Wrasse et al., 2006). Background wind in the direction of wave propagation is checked with the horizontal phase speed of the wave and we terminated the ray integration whenever it approaches the critical level. We calculated the wave action and thus the amplitude along the ray path by including the damping mechanisms. As information on wave amplitudes can not be unambiguously determined from the optical emission intensity measurements, we assumed the GW amplitude as unity (at 97 km) and traced back the relative amplitudes along the ray path. Further, as we have not considered the local time variation of the background parameters and thus, the ground-based wave frequency will be a constant. However, note that the intrinsic frequency still varies with altitude because of the varying background horizontal winds.

The observed and calculated GW parameters (intrinsic frequency, wave period, zonal, meridional, and vertical wave numbers) for all the wave events measured at the peak airglow emission altitudes as described in Sects. 2.1 and 2.2 are given as initial parameters to the ray tracing code. We considered all the different combinations of observed wave parameters including the errors in the observations for obtaining the ray paths and the uncertainties in them. Note that atmospheric tides have large amplitudes in the MLT region which, at times, can be of comparable sometimes to that of the background wind. As mentioned earlier, though tidal amplitudes are considered in the HWM-07 model, their day-to-day variability is not taken into account in the model. Amplitudes of the tides may reach as high as $20\,\mathrm{m\,s^{-1}}$ over equatorial latitudes (Tsuda et al., 1999). In order to account for the day-to-day variability of tidal amplitudes, we have included the tidal amplitudes of 5, 10, 15 K in T and 10, 20, 30 $\mathrm{m\,s^{-1}}$ in wind in

the model at 97 km as mentioned in Sect. 4. In general, above the stratopause, tidal amplitudes are large and increase exponentially with altitude. It is interesting to note that (figure not shown) the variabilities in the background atmospheric parameters developed with suite of instruments as mentioned above lies within the variability due to

5 tides. Ray path calculations are also carried out for these background profiles.

We traced the ray path using the above initial parameters from the initial latitude ($13.5° N/17.5° N$) and longitude ($79.2° E/78.5° E$) and altitude (97 km). The ray paths for the wave events G1 with the longitude-altitude, latitude-altitude and longitude-latitude are shown in Fig. 5a–c, respectively, for Gadanki and in Fig. 5d–f for (H1) Hyderabad.

10 Ray paths obtained while considering different background conditions (normal wind, zero wind and Gadanki model wind) and the day-to-day variability of tides are also superimposed with dotted lines. When we considered zero (Gadanki) wind, a shift of 71 km (25 km) in the horizontal position of the terminal point is observed with respect to that for normal wind for wave event G1. The shift reduced to 19 km and increased to

15 47 and 97 km when we considered the tidal variability of $+5$ K, $+10$ m s^{-1} and $+10$ K, $+20$ m s^{-1}, $+15$ K, $+30$ m s^{-1}, respectively, with respect to the normal wind. The shift is ~ 15 km for the tidal variability of -5 K, -10 m s^{-1}. The ray terminated in the mesosphere itself for tidal variability of -10 K, -20 m s^{-1} and -15 K, -30 m s^{-1} (figure not shown).

20 Over Hyderabad, for the wave event H1, shown in Fig. 5d–f, the shifts in the horizontal location of the terminal point are 305.6 km (148.7 km) for tidal variability of $+10$, $+20$ m s^{-1} (-10 K, -20 m s^{-1}), respectively, with reference to zero wind. This difference is only 59.5 km for tidal variability of -10 K, -20 m s^{-1} with respect to the normal wind. The terminal point locations for the rest of the wave events for normal winds are listed

25 in Table 1. Note that out of the five wave events over Gadanki two wave events (G3 and G4) got terminated in the upper mesosphere itself and one (G5) got terminated at 67 km. Over Hyderabad, out of the nine wave events, two wave events (H4 and H7) got terminated at ~ 67 km. In general, all the wave events which propagated down to the upper troposphere terminated between 10 and 17 km.

Profiles of square of vertical wave number (m^2), intrinsic frequency (ω_{ir}), Brunt Väiäsälä frequency (N), zonal, meridional, and vertical group velocity for event G1 are shown in Fig. 6a–f. Profiles of these parameters obtained for different background wind conditions (normal wind, zero wind, and Gadanki model wind) and the day-to-day vari-

5 ability of tides are also superimposed in the respective panels. The differences with and without the variability of tides in the above mentioned parameters are small below the stratopause, and are quite high above. Note that the effect of Doppler shifting of the wave frequency is larger at higher altitudes due to high wind amplitudes (Fig. 6b). Zonal group velocity shows (Fig. 6d) nearly the same behaviour as that of the zonal

10 wind. The intrinsic frequency, ω_{ir}, exceeded N at 13 km altitude and due to this m^2 became negative and the ray path got terminated there.

As mentioned earlier, the information on the wave amplitudes is not available from these instruments so we used the GW amplitude as unity and traced back the relative amplitudes along the ray path. Profiles of amplitudes of GWs observed for the wave

15 events G1 and H1 over Gadanki and Hyderabad are shown in Fig. 7a and b, respectively. Amplitudes with three different background wind conditions along with different tidal amplitudes are also shown in the respective panels. For unit wave amplitude near the observed region, it translates to 10^{-3} amplitude near the source region. Amplitude growth is found higher when either Gadanki or zero wind models were considered and

20 slightly lowered for the normal wind. They reduced much higher when we considered the tidal variability in the background wind. However, higher amplitude growth rates are observed over Hyderabad when we considered the normal wind along with tidal variability than zero wind. Similar growth rates were also observed for other wave events and are not shown here. Thus, background winds play a vital role in the growth rates

25 of GWs.

6 Identification of source(s) for the GW events

The geographical locations of the terminal points for different combinations of background winds along with different combinations of tidal variability are shown in Figs. 8 and 9 for Gadanki and Hyderabad wave events, respectively. In this figure, the contour encircling all the points (not drawn in the panels of the figure) represents the horizontal spread of uncertainty due to background conditions (including tidal variability). Terminal points of the rays (in the troposphere) are expected to be the location of GW sources. Since 9 out of 14 wave events got terminated between 10 and 17 km, we search for the possible sources around this altitude at the location. In general, major sources for the GW generation over tropics are orography, convection, and vertical shear in the horizontal winds. In the present case, GWs are unlikely to be generated by topography as the observed waves have phase speeds much greater than zero (Vadas et al., 2009). Tropical deep convection is assumed to be a major source for the generation of wide spectrum of GWs in the tropical latitudes. As mentioned earlier, OLR or IR BT is assumed to be proxy for the tropical deep convection. Lower the OLR/BT values, higher the cloud top and hence the deeper the convection. OLR (IRBT) $< 240\,\mathrm{W\,m^{-2}}$ (K) is taken to represent deep convection. It is quite logical to assume an absence of convection near-or-around the days of observation in-and-around Gadanki and Hyderabad, as the optical observations were obtained in clear sky conditions. However, convection may exist at locations away from the observational site and waves generated at those locations can propagate to the mesospheric altitudes over the site. In order to see the presence or otherwise of convection in the vicinity of the termination location, latitude-longitude cross section of NOAA interpolated OLR obtained for 17 March 2012 (8 March 2010) are shown in Fig. 8a (Fig. 9a) for Gadanki (Hyderabad) region. The terminal points of the rays for the wave events G1 and G2 (H1–H9 except H4 and H7) with different background wind conditions and different combinations of variability of the tides are also shown in the figure. As expected, no convection in-and-around Gadanki (Hyderabad) region can be noticed in this figure. Note that this plot

is with coarser grid (2.5° × 2.5° latitude-longitude) averaged for a day. The observed GWs could be generated due to localized sources having shorter temporal and spatial scales than those seen from the NOAA OLR data used. In order to check this, we have used IR BT data which is available at 4 km × 4 km grid size and at half an hour basis.

5 Latitude and longitude section of hourly IR BT at 14:00 (10:00), 15:00 and 16:00 UTC is shown in Fig. 8b–d (Fig. 9b), respectively. The terminal points with and without variability of tides are also shown. Interestingly no cloud patches can be seen at any of the times mentioned above. Thus, convection as a possible source for the observed wave events can be ruled out.

10   The other possible source for GW generation over this location is the vertical shear in the horizontal wind. The vertical shear in horizontal winds at an altitude of 10 km (8 km) on 17 March 2012 (8 March 2010) as a function of latitude-longitude is shown in Fig. 10a (Fig. 10b). The terminal points of the rays for both the wave events with and without the day-to-day variability of the tides are also shown in the figure. Interestingly,

15 at all the terminal points (in the troposphere), strong vertical shear in the horizontal wind which is quite high (8–$9\,\mathrm{m\,s^{-1}\,km^{-1}}$) is seen. In order to see whether these waves could be generated due to non-linear interaction (through Kelvin Helmholtz Instability, KHI), the Richardson number ($\mathrm{Ri} = \frac{N^2}{(\mathrm{d}U/\mathrm{d}z)^2}$) for this location is calculated (using ERA model) and is found to be $< 1/4$ showing that Ri satisfies the condition for instability.

20 Thus, the shear is unstable and hence conducive for the excitation of KHI leading to the generation of the propagating GWs through non-linear interaction. Note that shear excitation of the GWs has been examined theoretically using both linear and non-linear approaches (e.g., Fritts, 1982, 1984; McIntyre, 1978). For the excitation of radiating GWs by KH instabilities at a shear layer, the two mechanisms that are examined are

25 the vortex pairing (sub-harmonic interaction) and envelope radiation (Fritts, 1984). The vortex pairing is found to be highly dependent on the minimum Ri, whereas, the envelope radiation mechanism is found to provide efficient radiating wave excitation in the absence of propagating unstable modes (Fritts, 1984). Theoretical and numerical simulation work needs to be carried out to examine which of these mechanisms is effective

for the observed events in the present study. This aspect is beyond the scope of the present study and is planned to be taken up in the future.

Note that five wave events terminated at mesospheric altitudes. We examined the background atmospheric condition which can lead to the termination for these wave events at such high altitudes. The ray paths for two wave events observed on the same day over Gadanki could propagate down below with the same background atmosphere. When wave parameters related to this event are examined (Table 1) it can be seen that the phase speeds are small when compared to the other two wave events. When the wave is introduced at around 15 km with all the wave parameters similar to that observed at 97 km for this event and carried out forward ray tracing, it is seen that the ray propagated up to 50 km and terminating there. Note that strong vertical shear in the background wind is seen at this altitude (Fig. 3). To investigate the role of shear in the processes of propagation of waves, the shear was reduced to almost 0 in the 50–80 km altitude region. Under such conditions this wave event also could propagate to ~ 16 km (in the reverse ray tracing). This reveals that the background wind shear is obstructing the ray path. It is quite likely that the wave got ducted between 50 and 80 km and similar results are obtained for the other cases which got terminated in the mesosphere. This indicates that wind shears at mesospheric altitudes are responsible for termination at mesospheric altitudes for these events.

7   Summary and conclusions

Identification of the GW sources for the 14 wave events observed over Gadanki and Hyderabad using optical airglow measurements is presented. Reverse ray tracing method is developed to obtain the location of the source regions of the GWs in the troposphere/mesosphere. We made use of the MSISE-90 model for temperature and the HWM-07 for the zonal and meridional winds in addition to the ERA-Interim products in the lower atmosphere (1000 hPa to 1 hPa pressure levels), Gadanki climatological model, and zero wind model for the background atmosphere. We have incorporated

also the expected variability of tidal amplitudes of 5, 10, 15 K and 10, 20, 30 m s^{-1} in temperature and winds, respectively. There was an uncertainty of 50–100 and 150–300 km in the locations of terminal points when different wind and tidal variabilities are used. Wave action is successfully implemented taking into account the radiative and

5   diffusive damping. Considering the wave amplitude as unity at 97 km, amplitude of the wave is traced back to the source region for different wind models. Out of the 14 events examined, 9 ray paths terminated in the troposphere. The remaining 5 events got terminated in the mesosphere itself. We examined for possible sources for the 9 events for which the ray paths terminated in the troposphere.

10   Orography as the possible source was ruled out as wave events have high phase speeds. No tropical deep convection in-and-around Gadanki and Hyderabad was noticed near the ray terminal points. Interestingly, strong vertical shear in the horizontal wind is observed near the terminal points and these large shears are attributed to be the source for the GW events observed at the mesospheric altitudes. Examination of

15 the background wind conditions and wave parameters for the events that got terminated in the mesosphere revealed that the phase speeds were quite low for these strong vertical shears in the 50–80 km region (and at 95 km) resulted in the termination of the ray paths. It is likely that the waves generated in the troposphere are ducted between 50–80 km and the waves observed above this region are due to leakage of waves from

20 the duct. This aspect needs further investigation. Note that we have tested reverse ray tracing method successfully for fourteen wave events. Further, wave action is also implemented successfully by assuming the wave amplitudes as unity as information on the same is not available from optical observations. However, more number of cases are needed to be examined, particularly for the events that occur during Indian Summer

25 Monsoon season where convection and strong vertical shears in the horizontal winds co-exist due to prevailing tropical easterly jet (Venkat Ratnam et al., 2008). A few experiments are planned to conduct in the future at Gadanki by operating simultaneously MST radar, Radiosonde, Rayeligh Lidar, Airglow imager and Meteor radar which provides information right from the troposphere to the MLT region. Note that such a study

on the vertical propagation of meso-scale gravity wave from lower to upper atmosphere was made recently by Suzuki et al. (2013) using Airglow Imager and Lidar over Arctic region.

References

Alexander, M. J., Holton, J. R., and Durran, D. R.: The gravity wave response above deep convection in a squall line simulation, J. Atmos. Sci., 52, 2212–2226, 1995.

Alexander, M. J., Geller, M., McLandress, C., Polavarapu, S., Preusse, P., Sassi, F., Sato, K., Eckermann, S., Ern, M., Hertzog, A., Kawatani, Y., Pulido, M., Shaw, T. A., Sigmond, M., Vincent, R., and Watanabe, S: Recent developments in gravity-wave effects in climate models, and the global distribution of gravity-wave momentum flux from observations and models, Q. J. Roy. Meteor. Soc., 136, 1103–1124, 2010.

Brown, L. B., Gerrard, A. J., Meriwether, J. W., and Makela, J. J.: All-sky imaging observations of mesospheric fronts in OI 557.7 nm and broadband OH airglow emissions: analysis of frontal structure, atmospheric background conditions, and potential sourcing mechanisms, J. Geophys. Res., 109, D19104, doi:10.1029/2003JD004223, 2004.

Clark, T. L., Hauf, T., and Kuettner, J. P.: Convectively forced internal gravity waves: results from two-dimensional numerical experiments, Q. J. Roy. Meteor. Soc., 112, 899– 925, doi:10.1002/qj.49711247402, 1986.

Debashis Nath, Venkat Ratnam, M., Jagannadha Rao, V. V. M., Krishna Murthy, B. V., and Vijaya Bhaskara Rao, S.: Gravity wave characteristics observed over a tropical station using high-resolution GPS radiosonde soundings, J. Geophys. Res., 114, D06117, doi:10.1029/2008JD011056, 2009.

Dee, D. P., Uppala, S. M., Simmons, A. J., Berrisford, P., Poli, P., Kobayashi, S., Andrae, U., Balmaseda, M. A., Balsamo, G., Bauer, P., Bechtold, P., Beljaars, A. C. M., van de Berg, L., Bidlot, J., Bormann, N., Delsol, C., Dragani, R., Fuentes, M., Geer, A. J., Haimberger, L.,

Identification of gravity wave sources using reverse ray tracing over Indian region

M. Pramitha et al.

Title Page

Abstract	Introduction
Conclusions	References
Tables	Figures

◄	►
◄	►
Back	Close

Full Screen / Esc

Printer-friendly Version

Interactive Discussion

Healy, S. B., Hersbach, H., Hólm, E. V., Isaksen, L., Kållberg, P., Köhler, M., Matricardi, M., McNally, A. P., Monge-Sanz, B. M., Morcrette, J.-J., Park, B. K., Peubey, C., de Rosnay, P., Tavolato, C., Thépaut, J.-N., and Vitart, F.: The ERA-Interim-reanalysis: configuration and performance of the data assimilation system, Q. J. R. Meteor. Soc., 137, 553–597, 2011.

5 Dhaka, S. K., Choudhary, R. K., Malik, S., Shibagaki, Y., Yamanaka, M. D., and Fukao, S.: Observable signatures of a convectively generated wave field over the tropics using Indian MST radar at Gadanki (13.5° N, 79.2° E), Geophys. Res. Lett., 29, 1872, doi:10.1029/2002GL014745, 2002.

Drob, D. P., Emmert, J. T., Crowley, G., Picone, J. M., Shepherd, G. G., Skinner, W., Hays, P.,
10 Niciejewski, R. J., Larsen, M., She, C. Y., Meriwether, J. W., Hernandez, G., Jarvis, M. J., Sipler, D. P., Tepley, C. A., O'Brien, M. S., Bowman, J. R., Wu, Q., Murayama, Y., Kawamura, S., Reid, I. M., and Vincent, R. A.: An empirical model of the Earth's horizontal wind fields: HWM07, J. Geophys. Res., 113, A12304, doi:10.1029/2008JA013668, 2008.

Dutta, G., Ajay Kumar, M. C., Vinay Kumar, P., Venkat Ratnam, M., Chandrashekar, M.,
15 Shibagaki, Y., Salauddin, M., and Basha, H. A.: Characteristics of high-frequency gravity waves generated by tropical deep convection: case studies, J. Geophys. Res., 114, D18109, doi:10.1029/2008JD011332, 2009.

Eckermann, S. D.: Ray-tracing simulation of the global propagation of inertia gravity waves through the zonally averaged middle atmosphere, J. Geophys. Res., 97, 15849–15866,
20 1992.

Fovell, R., Durran, D., and Holton, J. R.: Numerical simulations of convectively generated stratospheric gravity waves, J. Atmos. Sci., 49, 1427–1442, 1992.

Fritts, D.C.: Shear excitation of atmospheric gravity waves, J. Atmos. Sci., 39, 1936–1952, 1982.

25 Fritts, D.C.: Shear excitation of atmospheric gravity waves, Part II: Nonlinear radiation from a free shear layer, J. Atmos. Sci., 41, 524–537, 1984.

Fritts, D. C. and Alexander, M. J.: Gravity wave dynamics and effects in the middle atmosphere, Rev. Geophys., 41, 1003, doi:10.1029/2001RG000106, 2003.

Fritts, D. C., Vadas, D. C. S. L., Wan, K., and Werne, J. A.: Mean and variable forcing of the
30 middle atmosphere by gravity waves, J. Atmos. and Sol. Terr. Phys., 68, 247–265, 2006.

Gerrard, A. J., Kane, T. J., Eckermann, S. D., and Thayer, J. P.: Gravity waves and mesospheric clouds in the summer middle atmosphere: a comparison of lidar measurements and ray

Identification of gravity wave sources using reverse ray tracing over Indian region

M. Pramitha et al.

modeling of gravity waves over Sondrestrom, Greenland, J. Geophys. Res., 109, D10103, doi:10.1029/2002JD002783, 2004.

Janowiak, J. E., Joyce, R. J., and Yarosh, Y.: A real-time global half-hourly pixel-resolution IR dataset and its applications, B. Am. Meteorol. Soc., 82, 205–217, 2001.

Hecht, J. H., Walterscheid, R. L., and Ross, M. N.: First measurements of the two-dimensional horizontal wave number spectrum from CCD images of the nightglow, J. Geophys. Res., 99, 11449–11460, 1994.

Hedin, A. E.: Extension of the MSIS thermosphere model into the middle and Lower atmosphere, J. Geophys. Res., 96, 1159–117, 1991.

Hocking, W. K.: The effects of middle atmosphere turbulence on coupling between atmospheric regions, J. Geomag., Geoelc., 43 (sup), 621–636, 1991.

Jones, W. L.: Ray tracing for internal gravity waves, J. Geophys. Res., 74, 2028–2033, 1969.

Kishore Kumar, G., Venkat Ratnam, M., Patra, A. K., Vijaya Bhaskara Rao, S., and Russell, J.: Mean thermal structure of the low-latitude middle atmosphere studied using Gadanki Rayleigh lidar, Rocket, and SABER/TIMED observations, J. Geophys. Res., 113, D23106, doi:10.1029/2008JD010511, 2008a.

Kishore Kumar, G., Venkat Ratnam, M., Patra, A. K., Jagannadha Rao, V. V. M., Vijaya Bhaskar Rao, S., Kishore Kumar, K., Gurubaran, S., Ramkumar, G., and Narayana Rao, D.: Low-latitude mesospheric mean winds observed by Gadanki mesosphere-stratosphere-troposphere (MST) radar and comparison with Rocket, High Resolution Doppler Imager (HRDI), and MF radar measurements and HWM93, J. Geophys. Res., 113, D19117, doi:10.1029/2008JD009862, 2008b.

Kumar, K. K.: VHF radar observations of convectively generated gravity waves: some new insights, Geophys. Res. Lett., 33, L01815, doi:10.1029/2005GL024109, 2006.

Kumar, K. K.: VHF radar investigations on the role of mechanical oscillator effect in existing convectively generated gravity waves, Geophys. Res. Lett., 34, L01803, doi:10.1029/2006GL027404, 2007.

Landau, L. D. and Lifshitz, E. M.: The Classical Theory of Fields, Pergamon, New York, 1962.

Laskar, F. I., Pallamraju, D., Vijaya Lakshmi, T., Anji Reddy, M., Pathan, B. M., and Chakrabarti, S.: Investigations on vertical coupling of atmospheric regions using combined multiwavelength optical dayglow, magnetic, and radio measurements, J. Geophys. Res., 118, 4618–4627, doi:10.1002/jgra.50426, 2013.

LeBlond, P. H. and Mysak, L. A.: Waves in the Ocean, Elsevier, New York, 1978.

Identification of gravity wave sources using reverse ray tracing over Indian region

M. Pramitha et al.

Lighthill, J.: Waves in Fluids, Vol. 1, Cambridge University, Press, London, 504 pp., 1978.

Lilly, D. K. and Kennedy, P. J.: Observations of a stationary mountain wave and its associated momentum flux and energy dissipation, J. Atmos. Sci., 30, 1135–1152, 1973.

Marks, C. J. and Eckermann, S. D.: A three-dimensional non-hydrostatic ray-tracing model for gravity waves: formulation and preliminary results for the middle atmosphere, J. Atmos. Sci., 52, 1959–1984, 1995.

McIntyre, M. E. and Weissman, M. A.: On radiating instabilities and resonant over-reflection, J. Atmos. Sci., 35, 1190–1196, 1978.

Mitchell, N. J. and Beldon, C. L.: Gravity waves in the mesopause region observed by meteor radar: 1. A simple measurement technique, J. Atmos. Sol. Terr. Phys., 71, 866–874, 2009.

Nakamura, T., Aono, T., Tsuda, T., Admiranto, A. G., and Achmad Suranto, E.: Mesospheric gravity waves over a tropical convective region observed by OH airglow imaging in Indonesia, Geophys. Res. Lett., 30, 1882–1885, 2003.

Narayana Rao, D., Ratnam, M. V., Rao, T. N., and Rao, S. V. B.: Seasonal variation of vertical eddy diffusivity in the troposphere, lower stratosphere and mesosphere over a tropical station, Ann. Geophys., 19, 975–984, doi:10.5194/angeo-19-975-2001, 2001.

Nastrom, G. D. and Fritts, D. C.: Sources of mesoscale variability of gravity waves I: Topographic excitation, J. Atmos. Sci., 49, 101–110, 1992.

Pallamraju, D., Laskar, F. I., Singh, R. P., Baumgardner, J., and Chakrabarti, S.: MISE: a multi-wavelength imaging spectrograph using echelle grating for daytime optical agronomy investigations, J. Atmos. Sol-Terr. Phys., 103, 176–183, 2013.

Pallamraju, D., Baumgardner, J., Singh, R. P., Laskar, F. I., Mendillo, C., Cook, T., Lockwood, S., Narayanan, R., Pant, T. K., and Chakrabarti, S.: Daytime wave characteristics in the mesosphere lower thermosphere region: results from the balloon-borne investigations of regional-atmospheric dynamics experiment, J. Geophys. Res., 119, 2229–2242, doi:10.1002/2013JA019368, 2014.

Piani, C., Durran, D., Alexander, M. J., and Holton, J. R.: A numerical study of three-dimensional gravity waves triggered by deep tropical convection and their role in the dynamics of the QBO, J. Atmos. Sci., 57, 3689–3702, doi:10.1175/1520-0469(2000)057<3689, 2000.

Schoeberl, M. R.: A ray tracing model of gravity wave propagation and breakdown in the middle atmosphere, J. Geophys. Res., 90, 7999–8010, doi:10.1029/JD090iD05p07999, 1985.

Title Page

Abstract	Introduction
Conclusions	References
Tables	Figures

|◄ | ►|

◄ | ►

Back | Close

Full Screen / Esc

Suzuki, S., Lubkena, F.-J., Baumgarten, G., Kaifler, N., Eixmann, R., Williams, B. P., and Naka-mura, T.: Vertical propagation of a mesoscale gravity wave from the lower to the upper atmo-sphere, J. Atmos. Sol. Terr. Phys., 97, 29–36, 2013.

Taori, A., Jayaraman, A., and Kamalakar, V.: Imaging of mesosphere–thermosphere airglow emissions over Gadanki (13.5° N, 79.2° E) – first results, J. Atmos. Sol. Terres. Phys., 93, 21–28, 2013.

Taylor, M. J., Pendleton, W. R. J., Clark, S., Takahashi, H., Gobbi, D., and Goldberg, R. A.: Image measurements of short-period gravity waves at equatorial latitudes, J. Geophys. Res., 102, 26283–26299, 1997.

Tsuda, T., Ohnishi, K., Isoda, F., Nakamura, T., Vincent, R. A., Reid, I. M., Harijono, S. W. B., Sribimawati, T., Nuryanto, A., and Wiryosumarto, H.: Coordinated radar observations of at-mospheric diurnal tides in equatorial regions, Earth Planets Space, 51, 579–592, 1999.

Vadas, S. L., Taylor, M. J., Pautet, P.-D., Stamus, P. A., Fritts, D. C., Liu, H.-L., São Sabbas, F. T., Rampinelli, V. T., Batista, P., and Takahashi, H.: Convection: the likely source of the medium-scale gravity waves observed in the OH airglow layer near Brasilia, Brazil, during the Spread-FEx campaign, Ann. Geophys., 27, 231–259, doi:10.5194/angeo-27-231-2009, 2009.

Venkat Ratnam, M., Narendra Babu, A., Jagannadha Rao, V. V. M., Vijaya Baskar Rao, S., and Narayana Rao, D.: MST radar and radiosonde observations of inertia-gravity wave climatology over tropical stations: source mechanisms, J. Geophys. Res., 113, D07109, doi:10.1029/2007JD008986, 2008.

Vincent, R. A. and Alexander, M. J.: Gravity waves in the tropical lower stratosphere: an obser-vational study of seasonal and interannual variability, J. Geophys. Res., 105, 17971–17982, 2000.

Wrasse, C. M., Nakamura, T., Tsuda, T., Takahashi, H., Medeiros, A. F., Taylor, M. J., Gobbi, D., Salatun, A., Suratno, Achmad, E., and Admiranto, A. G.: Reverse ray tracing of the meso-spheric gravity waves observed at 23° S (Brazil) and 7° S (Indonesia) in airglow imagers, J. Atmos. Sol. Terr. Phys., 68, 163–181, 2006.

Zhu, X.: Radiative damping revisited: parameterization of damping rate in the middle atmo-sphere, J. Atmos. Sci., 50, 3008–3012, 1993.

Title Page

Abstract | Introduction

Conclusions | References

Tables | Figures

|◄ | ►|

◄ | ►

Back | Close

Full Screen / Esc

Printer-friendly Version

Interactive Discussion

Table 1. GW characteristics (direction of propagation (ϕ), horizontal wavelength (λ_h), period (T), phase speed (C) and intrinsic frequency (ω_{ir})) for events observed over Gadanki (G) and Hyderabad (H). The terminal point locations (latitude, longitude and altitude) are also shown for each event. Conditions leading to the termination for each wave event are also shown. Events for which ray paths terminated at mesospheric altitude are indicated with an asterisk.

Events	ϕ (degrees)	λ_h (km)	T (min)	C (m s^{-1})	Longitude (degrees)	Latitude (degrees)	Altitude (km)	ω_{ir} (rad s^{-1})	Termination condition
Gadanki location									
G1	102	85	18	78	79.9	10.8	13	0.00058	$m^2 < 0$
G2	98	34	9	63	79.4	12.3	17	0.0116	$m^2 < 0$
G3	132	12	6	33	79.2	13.37	96.9*	0.0006	Intrinsic frequency approaching zero
G4	62	134	12	186	79.14	13.2	92.9*	0.0093	WKB > 1
G5	142	16	8	33	79.9	12.7	66.9*	0.0156	WKB > 1 and $m^2 < 0$
Hyderabad location									
H1	11	39	16	41	70.2	15.8	10.5	0.0028	WKB > 1
H2	16	57	16	59	75.3	16.4	13.5	0.0046	WKB > 1
H3	21	74	16	77	75.9	16.3	14.5	0.0049	WKB > 1
H4	11	39	20	32.5	76.3	17.1	67.6*	0.00083	$m^2 <$ limiting condition and intrinsic frequency approaching zero
H5	16	57	20	48	72.7	15.7	12.5	0.0029	WKB > 1
H6	21	74	20	61.7	74.7	15,8	13.5	0.0035	WKB > 1
H7	11	39	23	28	75.8	16.9	68.5*	0.00087	$m^2 <$ limiting condition and intrinsic frequency approaching zero
H8	16	57	23	41	68.3	14,8	11.5	0.0022	WKB > 1
H9	21	74	23	54	73.4	15.4	13.5	0.0032	WKB > 1

Table 2. Details of instruments, parameters measured, altitude range in which data is available and the duration of the data considered for developing the Gadanki atmospheric model.

Instrument (parameter(s) obtained)	Altitude range covered	Duration of the data considered
Indian MST radar (U, V)	4–21 and 65–85 km	1996–2012
Radiosonde (U, V, T)	1–30 km	2006–2012
Lidar (T)	30–75 km	1998–2012
Rocket (U, V, T)	22–80 km	1970–1991, 2002–2007
HALOE, HRDI/UARS (T, U, V)	65–110 km	1991–2000
SABER/TIMED (T)	30–110 km	2002–2012

Figure 1. Identification of three wave events (left to right) obtained from the airglow emission intensities originating from $O(^1S)$ emissions from Gadanki. The wave crests are emphasized by yellow freehand lines. Motion of waves can be obtained by successive images and the direction of propagation is shown by red arrows. Time of occurrence of events is shown in each image in UTC (hh:mm).

Figure 2. Climatological monthly mean contours of **(a)** temperature, **(b)** zonal wind and **(c)** meridional wind obtained over Gadanki region combining a variety of instruments listed in Table 2.
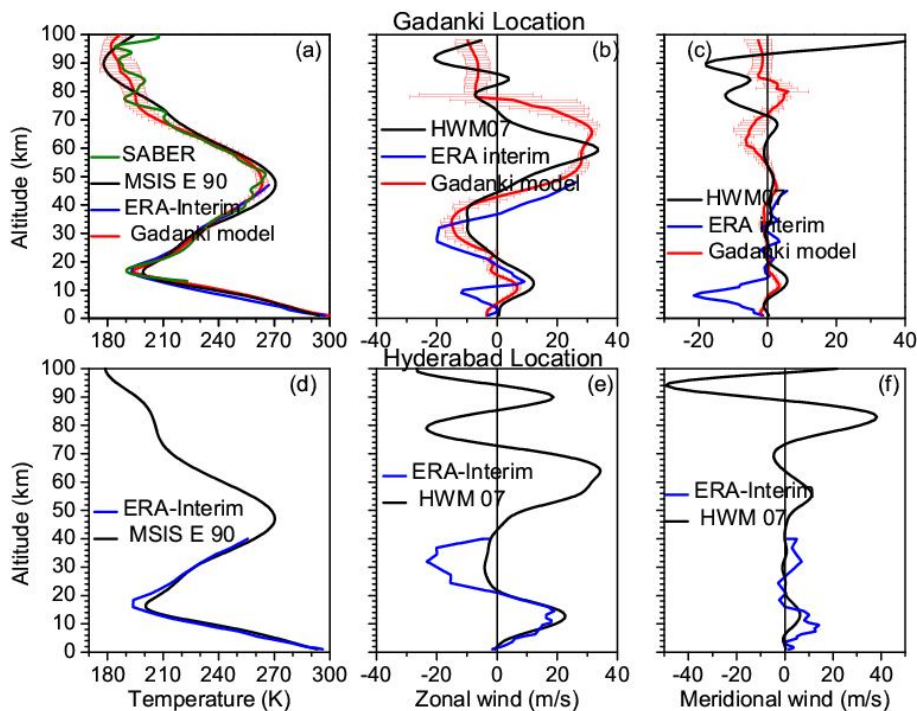
Figure 3. Profiles of **(a)** temperature **(b)** zonal wind and **(c)** meridional wind obtained using ERA-interim data products for 17 March 2012, 12:00 UTC over Gadanki region. Profiles obtained from variety of sources over Gadanki (Gadanki model) listed in Table 2 are also superimposed in the respective panels for comparison. Plots **(d–e)** are same as **(a–c)** but obtained for Hyderabad on 8 March 2010. Temperature profile obtained from MSISE-90 and zonal and meridional winds obtained from HWM 07 for the same day are also provided in the respective panels.
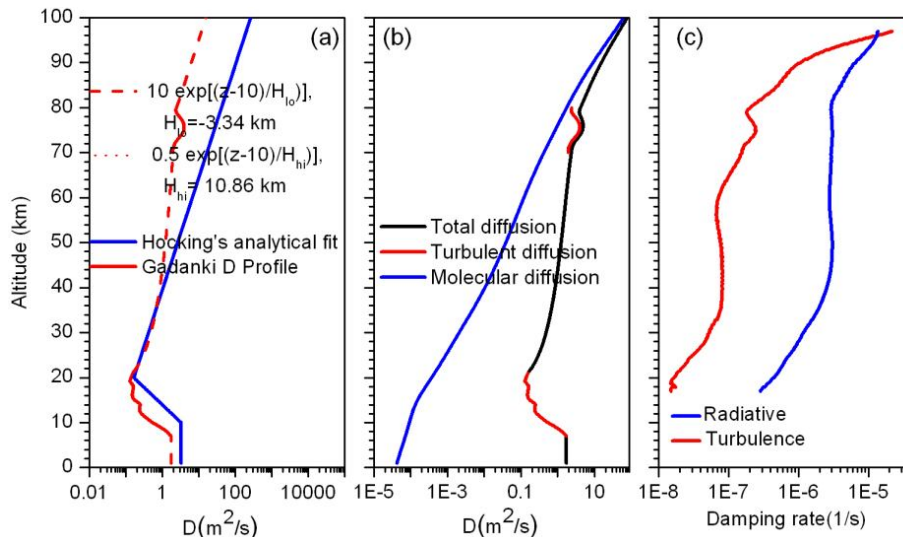
Figure 4. (a) Profile of eddy diffusitvity (thick red line) obtained from Gadanki MST radar (Rao et al., 2001) in the tropopshere, lower stratopshere and mesopshere. Fitted profile (dotted line) with exponetial function is also shown. Hocking's (Hocking 1991) analytical curve (extrapolated) is also superimposed for comparsion. **(b)** Profiles of eddy, molecualr, and total diffusivity. **(c)** Radiative, and diffusive damping rates.
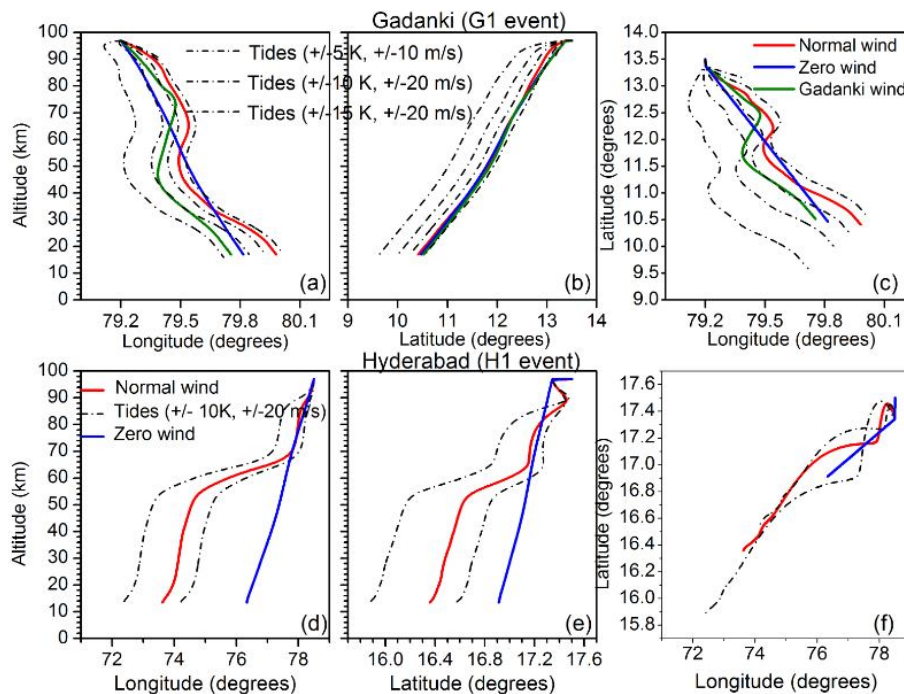
Figure 5. Ray paths for the wave event G1 in the **(a)** longitude–altitude, **(b)** latitude–altitude, and **(c)** longitude–latitude cross sections. Ray paths obtained while considering different background wind conditions (normal wind, zero wind and Gadanki model wind) and the day-to-day variability of tides are also superimposed (dotted lines). **(d–f)** same as **(a–c)** but for the wave event H1. Note that Gadanki atmospheric model wind is not used for the wave events over Hyderabad.
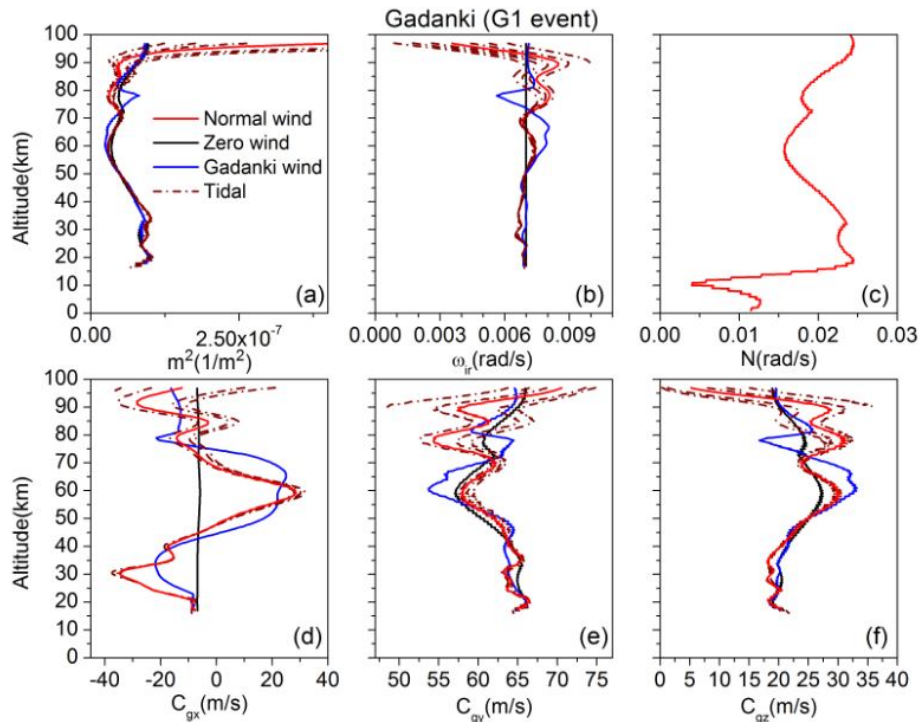
Figure 6. Profiles of **(a)** square of vertical wave number (m^2), **(b)** intrinsic frequency (ω_{ir}), **(c)** Brunt Väisälä frequency (*N*), **(d)** zonal, **(e)** meridional, and **(f)** vertical group velocities for the wave event G1. Profiles of the same obtained while considering the three different background winds (different coloured lines) and the day-to-day variability of tides are also superimposed (dotted lines) in the respective panels.
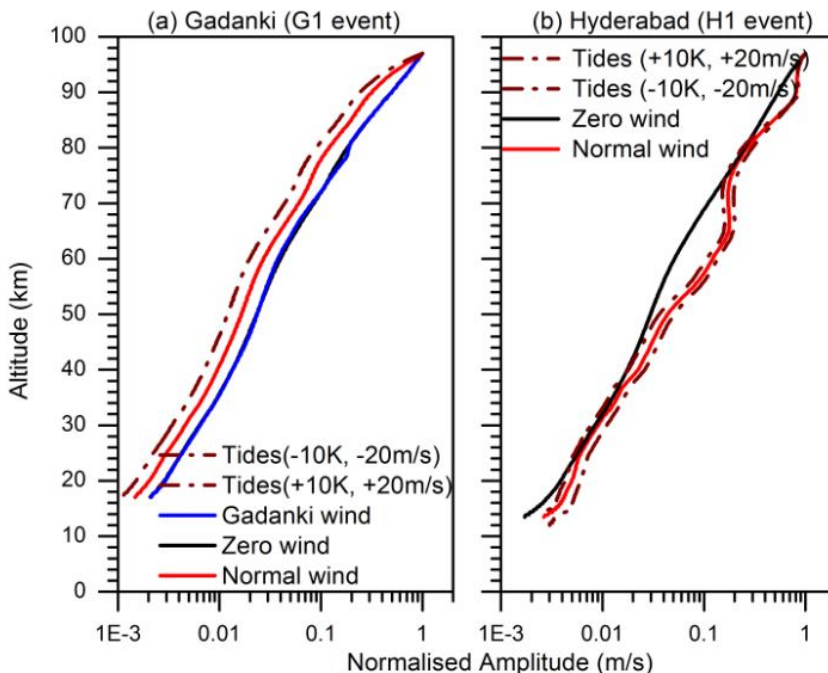
Figure 7. Normalised amplitudes of gravity waves observed for the wave events **(a)** G1, and **(b)** H1, over Gadanki and Hyderabad, respectively. Amplitudes with three different background wind conditions along with different tidal amplitudes are also shown.
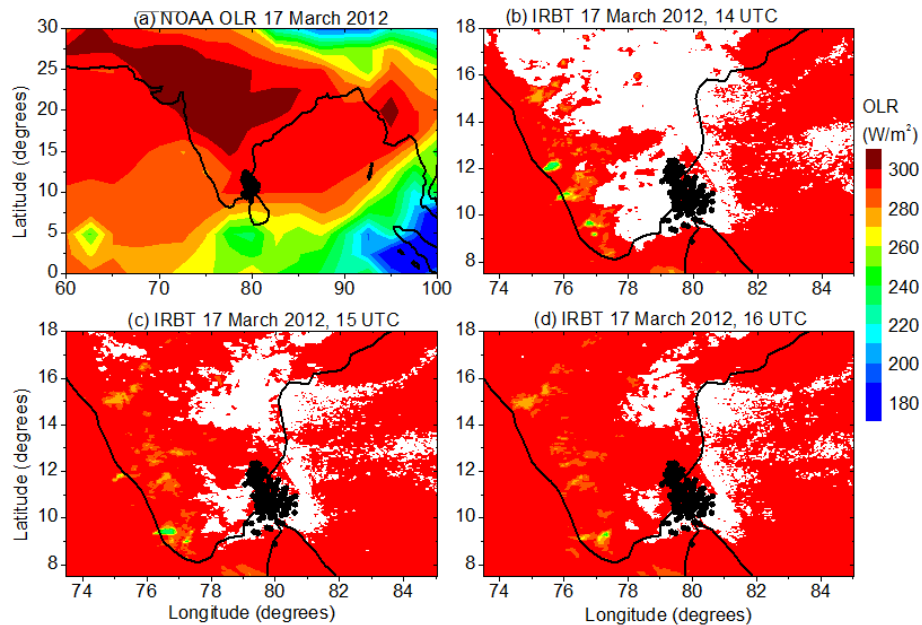
Figure 8. Daily mean latitude-longitude section of **(a)** OLR observed using NOAA products over Indian region on 17 March 2012. **(b–d)** same as **(a)** but for IRBT observed at 14:00, 15:00, and 20:00 UTC, respectively. Open (closed) circles in **(a)–(d)** depict the terminal points of the ray paths shown in Fig. 5.
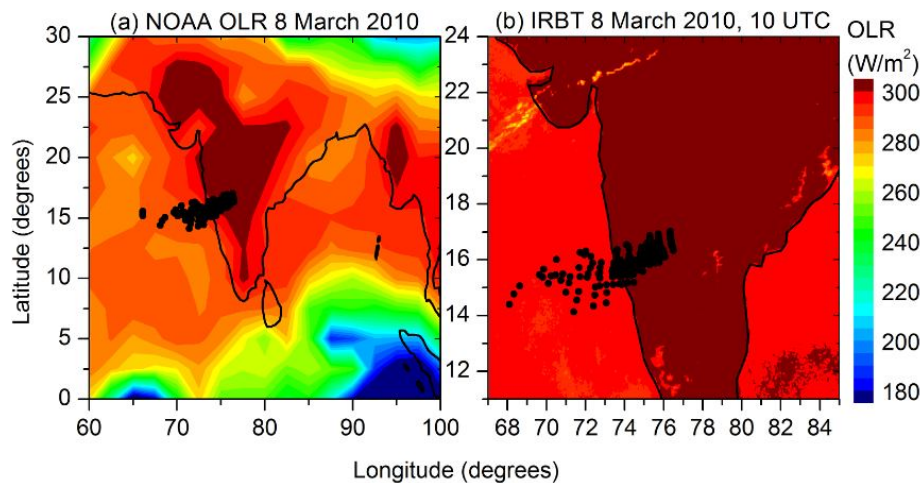
Full Screen / Esc

Figure 9. Same as Fig. 8 but for wave events observed over Hyderabad on 8 March 2010. Note that IRBT is shown only for 10:00 UTC.

Full Screen / Esc

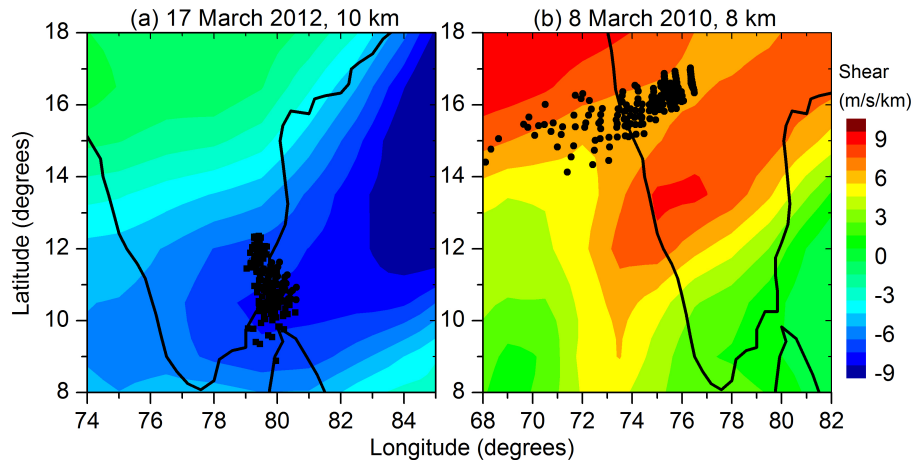Printer-friendly Version

Interactive Discussion

Figure 10. Latitude-longitude section of vertical shear in the horizontal wind observed using ERA-Interim data products on **(a)** 17 March 2012 at 10 km, **(b)** 8 March 2010 at 8 km. Filled circles depicts the terminal points of the ray paths estimated using three different wind conditions and tidal amplitudes.